## PAPER

Check for updates

# A combined photoelectron-imaging spectroscopic and theoretical investigation on the electronic structure of the VO₂H anion

Yongtian Wang,[a] Changcai Han,[ab] Jing Hong,[ab] Zejie Fei,[a] Changwu Dong, ⓘD *[a] Hongtao Liu*[a] and Xiaogen Xiong[c]

The electronic structure and vibrational spectrum of the VO₂H anion are explored by combining photoelectron imaging spectroscopy and density functional theoretical (DFT) calculations. The electron affinity (EA) of VO₂H is determined to be 1.304 ± 0.030 eV from the vibrationally resolved photoelectron spectrum acquired at 1.52 eV (814 nm). The anisotropy parameter ($\beta$) for the EA defined peak is measured to be 1.63 ± 0.10, indicating that it is the 17a′ (4s orbital of the vanadium atom) electron attachment leading to the formation of the ground state of the VO₂H anion. The vibrational fundamentals $\nu_1$, $\nu_3$, $\nu_4$ and $\nu_5$ are obtained for the neutral ground state. Experimental assignments are confirmed by energies from electronic structure calculations and Franck–Condon (FC) spectral simulations. These simulations support assigning the anion ground state as the results obtained from the B3LYP method. In addition, the molecular orbitals and bonding involved in the anionic VO₂H cluster are also examined based on the present theoretical calculations.

## 1. Introduction

Vanadium oxides play a tremendous role in heterogeneous catalysis. Bulk or supported vanadium oxides are employed as catalysts in a number of industrial catalytic reactions aimed at energy sustainability, such as the oxidation of SO₂ to SO₃ in the production of sulfuric acid, oxidation of butene to phthalic anhydride and selective reduction of NO$_x$ with NH₃.[1–6] Exploring the structure and active sites of vanadium oxide catalysts is the key to understanding the catalytic mechanisms and designing catalysts. However, the investigations of detailed catalytic mechanisms in solid state and aqueous media are often hampered due to the complicated surface properties and environments, such as the inhomogeneity and surface defects of the catalyst, rapid aggregation, solvent effects and others. Gas-phase studies of isolated vanadium oxides can reveal molecular-insights into electronic structures of catalysts and reaction mechanisms in precisely controlled conditions. In addition, the discovery of new catalytic models in the gas phase can feed back to the design of bulk catalysts.

The oxidation of the alcohols is important for more valuable industrial products such as formaldehyde, dimethylether, methyl-*t*-butylether and even biodiesel.[1,7,8] Vanadium oxides catalysts are employed in a variety of catalytic oxidation processes of significant importance to these chemical industries. Therefore, the studies on reactivity of a range of vanadium oxides with the alcohols are the focus of sustained research efforts.[3–5] Besides, alcohols and alkoxides have been proposed as intermediates in other oxidation reactions mediated by vanadium oxides.[9,10] Both theoretical calculations[11–15] and experimental methods[16–25] are employed to study the dehydrogenation of alcohols by vanadium oxides in the gas phase. Most of these studies have focused on the reactivity of neutral and cationic vanadium oxides with alcohols, but few on anionic vanadium oxides as catalysts. Tom Waters and co-workers described the gas-phase catalytic oxidation of methanol to formaldehyde with the anion VO₃⁻ as catalyst and found that a key step in the process was the reaction of VO₃⁻ with methanol to eliminate water.[19] An experimental investigation of the gas-phase ion/molecule reactions of VO₂⁺ with a variety of alcohols shows that VO₂⁺ induce an oxidative dehydrogenation of alcohols.[16] The neutral VO₂ clusters can abstract more than one hydrogen atom from CH₃ and/or OH moiety of CH₃OH to form VO₂H₁,₂ products.[20] Although many studies on reactivity of vanadium oxides with the alcohols in the gas-phase have been done, there are few acknowledgements on electronic structure and spectrum information of these reaction products.

In the present work, we characterize gas-phase VO₂H⁻ using photoelectron spectroscopy (PES) and density functional theory (DFT) approaches. Over the last few decades, the molecular structure and several low-lying electronic states of neutral and

*[a]Key Laboratory of Interfacial Physics and Technology, Shanghai Institute of Applied Physics, Chinese Academy of Sciences, Shanghai 201800, P. R. China. E-mail: dongchangwu@sinap.ac.cn; liuhongtao@sinap.ac.cn*

*[b]University of Chinese Academy of Sciences, Beijing 100049, P. R. China*

*[c]Sino-French Institute of Nuclear Engineering and Technology, Sun Yat-sen University, Zhuhai 519082, P. R. China*

anion $VO_2^-$ had been clearly determined by other groups using anion photoelectron spectroscopy experiments and advanced theoretical calculations.[26–30] Here, we obtain the vibrationally resolved photoelectron imaging spectroscopy of $VO_2H^-$ firstly, which is the product of the dehydrogenation of ethanol mediated by $VO_2^-$. The assignments of electronic configuration and vibration are all performed with the aid of electronic structure calculation and frequency analysis. The electronic configuration similarity between $VO_2H^-$ and $VO_2^-$ were also described.

## 2. Experimental and computational methods

### Experimental methods

The experiment was performed using a home-built instrument with a laser vaporization source, a time-of-flight mass spectrometer coupled with velocity-map imaging (VMI) spectrometer. The apparatus have been described in detail elsewhere,[31] and only a brief outline is given below. The $VO_2^-$ and $VO_2H^-$ anions were produced from the laser vaporization process in a supersonic expansion of the Ar/He (5%/95%) carrier gas carrying traces of ethanol at 6 atm. The second harmonic generation of Nd:YAG laser (Continuum, Minilite II) at 532 nm was used to vaporize the vanadium metal target. The anions were cooled and expanded into the McLaren–Wiley time-of-flight mass spectrometer.[32] After assignment of anions, the anionic clusters of interest were mass selected into the photodetachment region and crossed with a dye laser beam, which (Spectra-Physics, 400–920 nm, linewidth 0.06 cm$^{-1}$ at 625 nm) was pumped by a Nd:YAG laser (Quanta-Ray Pro 190, 10 Hz). The detached photoelectrons were extracted by a velocity-map imaging photoelectron spectrometer and recorded by a charge-coupled device camera. Each image was obtained by 5000–50 000 laser shots at 10 Hz repetition rate. The raw imaging stands for the projection of the photoelectron density in the 3D laboratory frame on the 2D imaging detector. The original 3D distribution was reconstructed using the Maximum Entropy Velocity Legendre Reconstruction (MEVELER) technique.[33] The known transitions from the detachment of the Au$^-$ are used to calibrate all images.[34] The energy resolution was 30 meV at an electron kinetic energy (eKE) of 1 eV. Spectra are plotted as a function of the electron binding energy (eBE) given by eBE = $h\nu$ − eKE.

### Computational methods

Calculations of the optimized geometries and electronic structures of the anionic and neutral $VO_2H$ clusters were accomplished using the Gaussian 09 program.[35] Different spin multiplicity states of the clusters were attempted to determine the ground-state geometries. The structures were fully optimized without symmetry constraints. In this study, the BP86 (ref. 36 and 37) and B3LYP[38] density functionals methods were employed to optimize the lowest-energy geometries and to estimate the electronic affinity (EA) energy, that is adiabatic detachment energy (ADE), of the anionic $VO_2H$ cluster. Throughout the calculations, the augmented correlation

consistent triple-zeta (aug-cc-pVTZ) basis set was adopted for the oxygen and hydrogen atoms,[39] while the vanadium atomic orbital was described by the triple-zeta LANL2TZ basis set combined with the Hay and Wadt effective core potentials.[40,41] Moreover, vibration analyses were performed at the same level of theory to make sure that the optimized geometries are real minimum points and to take into account the zero-point energy (ZPE) correction. The theoretical EA value was defined as the energy difference between the optimized anionic and neutral structures under considering the ZPE correction, and the VDE was calculated by considering the energy difference between the ground-state of the anion and neutral cluster with the equilibrium geometry of the anion.

## 3. Results and discussion

### Mass spectrum and PES

As shown in Fig. 1(a), the $m/z$ of predominate anionic species is 83 corresponding to $VO_2^-$, which probably was generated from the oxide on the surface of vanadium metal rod. The $m/z$ of 67, 68, 69, 84 and 85 corresponding to $VO^-$, $VOH_{1,2}^-$ and $VO_2H_{1,2}^-$ were also observed, but these peaks are much weaker than that of $VO_2^-$. The observed weak signal of $VO_2H^-$ should arise from the reaction between $VO_2$ and $H_2O$ molecules that remain in the source chamber, since the carrier gas is only Ar/He (5%/95%). When trace ethanol was added in the carrier gas Ar/He, some new characters were observed in the mass spectrum. As shown in Fig. 1(b), the mass signal of $VO_2H^-$ noticeably enhanced, was almost equal strength as that of $VO_2^-$. It is obvious that the $VO_2^-$ combines very easily with the hydrogen atoms in the ethanol to form $VO_2H^-$. Some new weak mass peaks were also produced, the $m/z$ of 76, 77 and 78 corresponding to $VC_2H_x^-$ ($x$ = 1–3). The $m/z$ of 81 and 82 was assigned to peaks of $V(CH_3)_2$/$VOCH_2$ and $VOCH_3$ anions. However, these mass peaks were too weak to obtain their photoelectron spectra.

Fig. 2 depicts the photoelectron image and corresponding PES of $VO_2H^-$ cluster obtained at a photon energy of 1.52 eV (814 nm). In the present experiment, the laser polarization,
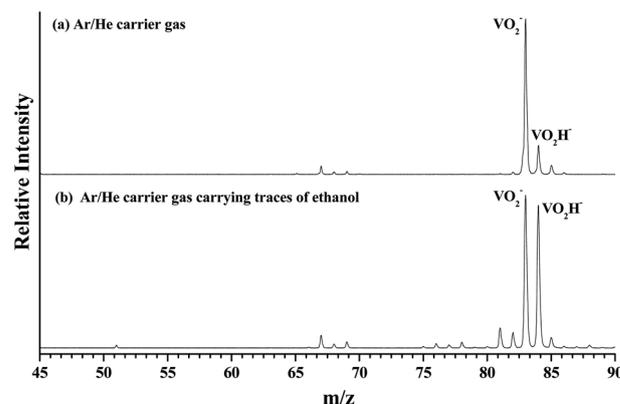


**Fig. 1** The mass spectrum of laser vaporizing the vanadium metal at 532 nm. (a) Displays the anionic cluster distribution generated by Ar/He (5%/95%) expansion gas, (b) displays the new cluster distribution after Ar/He (5%/95%) expansion gas carrying trace of ethanol.
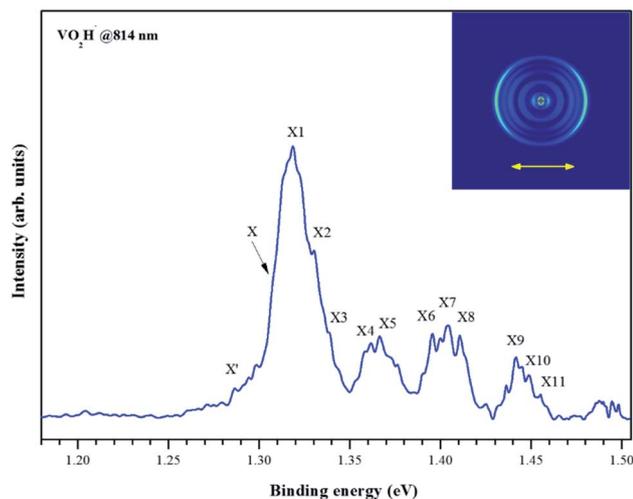
Fig. 2 Photoelectron image and the corresponding electron binding energy (eBE) spectrum of the negatively charged VO$_2$H cluster collected at 814 nm.

which is represented by a double black arrow, is parallel to the photoelectron angular distribution (PAD) of the peak X. The collected PES of VO$_2$H$^-$ shows a series of broad peaks, which corresponding to the excited vibrational transition, arising from the transition between the ground state of VO$_2$H$^-$ and its corresponding neutral electronic ground state. The EA of 1.304 ± 0.030 eV is deduced from the right shoulder of the strongest peak, and labeled as X. The VDE of 1.317 ± 0.030 eV is obtained from the position of strongest peak and labeled as X1. In addition, four vibrational progressions can be observed in this spectrum. The first progression is comprised from the equally spaced peaks X1–X3, equally spacing is about 100 cm$^{-1}$, and offset by 104 cm$^{-1}$. The peaks X4 and X5 comprise the second progression, and this progression is offset by about 460 cm$^{-1}$. The third progression is offset by 734 cm$^{-1}$, and comprised by peaks X6–X8, and these peaks are spacing by ∼60 cm$^{-1}$. The peaks X9–X11 comprise the forth progression, which is offset by 1065 cm$^{-1}$, the equally peaks spacing is also around 60 cm$^{-1}$.

The peak X′ is assigned to the hot band, arising from the mode 1 vibration in the ground state of VO$_2$H$^-$ excited to its corresponding neutral electronic ground state, this frequency is about 137 cm$^{-1}$. Peak positions (eBE) and assignments are summarized in Table 1. The peaks are wider than the instrumental resolution owing to unresolved rotational structure and the hot band broadening in the cluster source beam.

One of the advantages of the photoelectron imaging technique is to obtain the PAD of the detached electron. For one-photon detachment, the PAD is given by the form,

$$\frac{d\sigma}{d\Omega} = \frac{\sigma_{tot}}{4\pi}\left(1 + \beta\left(\frac{3}{2}\cos^2\theta - \frac{1}{2}\right)\right) \quad (1)$$

where $\theta$ is the angle of the ejected electron relative to the polarization of the photodetachment laser. The anisotropy parameter $\beta$ varies from −1 to 2, corresponding to the limit where the electron distribution is aligned perpendicular and parallel to the laser polarization.[42,43] In molecular systems, it is well-accepted that detachment from the σ molecular orbital composed predominantly of atomic s-type character will produce anisotropy parameter of $\beta \sim 1.5$–2.[44] The experimentally measured $\beta$ value associated with the X peak is 1.63 ± 0.10, demonstrating that the detachment process should occur from the σ molecular orbital and the ground state of VO$_2$H$^-$ is X $^4$A″ state.

## Cluster geometry and electronic structure calculations

The metal oxide systems are often formally considered ionic, however covalent molecular orbital theory has proven to be a useful framework for understanding the electronic structure of the 3d transition metal monoxides,[45,55] and is used here for elucidating the relevant electronic states of the neutral and anionic VO$_2$H cluster. The ground state electronic configuration of atomic V is 4s$^2$3d$^3$. In the VO$_2$H and VO$_2$H$^-$, the formal oxidation state of the vanadium atom is +3 and +2, leaving two and three metal-centered valence electrons in the neutral and anion, respectively.

Earlier theoretical studies of vanadium oxides clusters have used the B3LYP and BP86 density functionals to obtain

Table 1 Peak positions (eV), shifts from respective origins (eV), and vibration assignments for the VO$_2$H$^-$ PES spectra

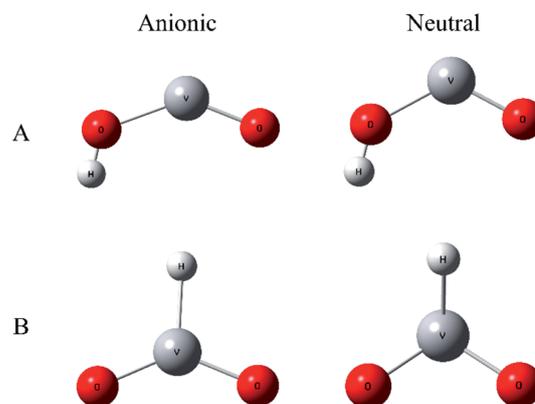| Peak | eBE | Offset | Assignment |
|------|------|--------|------------|
| X′ | 1.287 | 0.017 | $1_1^0$ |
| X | 1.304 | 0 | $0_0^0$ |
| X1 | 1.317 | 0.013 | $1_0^1$ |
| X2 | 1.330 | 0.026 | $1_0^2$ |
| X3 | 1.343 | 0.039 | $1_0^3$ |
| X4 | 1.361 | 0.057 | $3_0^1$ |
| X5 | 1.367 | 0.063 | $1_0^1 3_0^1$ |
| X6 | 1.395 | 0.091 | $4_0^1$ |
| X7 | 1.404 | 0.100 | $1_0^1 4_0^1$ |
| X8 | 1.411 | 0.107 | $1_0^2 4_0^1$ |
| X9 | 1.436 | 0.132 | $5_0^1$ |
| X10 | 1.441 | 0.137 | $1_0^1 5_0^1$ |
| X11 | 1.449 | 0.145 | $1_0^2 5_0^1$ |



Fig. 3 The structures scheme of A and B isomers of VO$_2$H cluster in the anionic and neutral states.

**Table 2** Theoretical relative energies $\Delta E$, EA and VDE for different spin multiplicities of the neutral and anionic VO$_2$H clusters calculated at the DFT level of theory

| Species | Isomer | Spin multiplicity | $\Delta E$ (eV) | EA (eV) | VDE (eV) |
|---|---|---|---|---|---|
| **B3LYP/LANL2TZ** | | | | | |
| VO$_2$H$^-$ | A | 2 | 1.14 | 1.75 | 2.08 |
| | | 4 | 0.85 | 1.39 | 1.49 |
| | B | 2 | 0.00 | 2.74 | 3.22 |
| | | 4 | 2.55 | 2.10 | 2.43 |
| VO$_2$H | A | 1 | 0.94 | | |
| | | 3 | 0.00 | | |
| | B | 1 | 0.15 | | |
| | | 3 | 2.21 | | |
| **BP86/LANL2TZ** | | | | | |
| VO$_2$H$^-$ | A | 2 | 1.14 | 1.99 | 2.13 |
| | | 4 | 0.85 | 1.33 | 1.49 |
| | B | 2 | 0.00 | 2.33 | 2.62 |
| | | 4 | 2.55 | 1.84 | 2.18 |
| VO$_2$H | A | 1 | 0.94 | | |
| | | 3 | 0.00 | | |
| | B | 1 | 0.15 | | |
| | | 3 | 2.21 | | |

geometries, electronic states, and vibrational frequencies. B3LYP was successfully used in comparison with experimental IRPD results of various vanadium oxide clusters.[46] BP86 was used to predict the electronic and structural properties of VO$_2$ clusters.[47] Many different density functional methods, including BPW91, has been made on the relative merits of different functionals, although it is believed that pure density functionals like BP86 and BPW91 are more reliable for multi-reference systems than B3LYP, which includes some Hartree–Fock exchange.

To improve confidence in the theoretical results, both the B3LYP and BP86 functionals are used to calculate the anion and neutral VO$_2$H$^-$ energies, geometries, and vibrational frequencies. The geometries optimization gives two stable conformation in neutral and anionic ground state, as shown in Fig. 3. In isomer A, hydrogen atom combined with O atom form a planar $C_s$ symmetry, and in isomer B, the hydrogen atom coordinated with center vanadium atom. Previous calculations and

experiments found that neutral VO$_2$ was doublet in ground state,[48] meanwhile the anion VO$_2^-$ has been assigned to be triplet in ground state. In VO$_2$H cluster, the additional hydrogen 1s electron will change the spin multiplicity to singlet or triplet in neutral ground state, and to doublet or quartet in anionic ground state. Different spin states of the clusters were calculated, and the theoretical results are listed in Table 2. As shown in Table 2, the present calculations predict a triplet state as the global minimum of VO$_2$H isomer A, while that of VO$_2$H$^-$ isomer B has a doublet spin multiplicity, however only the EA predicted from a triplet state of neutral and a quartet state of anionic VO$_2$H cluster for isomer A supports the experimentally assigned that of VO$_2$H$^-$ discussed above.

The theoretical equilibrium geometries parameters of isomer A are listed in Table 3. It is necessary to note that the bond length of V–O$_\alpha$, in which the oxygen atom is bonded to the hydrogen atom, is longer than that of V–O$_\beta$, in which the oxygen atom is on the other side of the cluster, by 0.2–0.3 Å for both anionic and neutral VO$_2$H cluster. That means the interaction between O and H atom much more weakens the strength of V–O bond. When electron was detached, H–O bond length is not changed obviously, but bond angle $\theta$ of OVO is changed in different trend for B3LYP and BP86 methods. In B3LYP method, the $\theta$ value is enlarged from 144.1° to 155.9°, while that is decreased from 137.5° to 122.9° under BP86 theory. This should be due to the different methods giving the different ground-state electronic configuration.

With the aid of optimized ground-state geometries of the neutral and anionic V$_2$OH clusters, we can theoretically predict the EA values of the V$_2$OH$^-$ cluster, which can be used to compare with the experimentally determined data. Such a comparison is of great value to test the accuracy of the chosen theoretical method and optimized geometries. Additionally, as other investigations earlier, it is a challenge to precisely predict the EA of VO$_2$H since there are relatively large differences between previous experiment and theory on VO and VO$_2$ clusters.[47–50] It has been demonstrated and emphasized that the energy levels of transition metal doped clusters are very sensitive to the choice of the level of theory and basis set.[51] Therefore, apart from determining the ground state of VO$_2$H$^-$, another motivation of the present study is to explore the appropriate

**Table 3** Theoretical equilibrium bond lengths $R$, bond angle $\theta$ and dihedral angle $\varphi$ for isomer A of the neutral and anionic VO$_2$H clusters calculated at the DFT level of theory

| Species | Spin multiplicity | $R_{V-O_\alpha}{}^a$ (Å) | $R_{V-O_\beta}{}^a$ (Å) | $R_{H-O_\alpha}$ (Å) | $\theta^b$ (deg) | $\varphi$ (deg) |
|---|---|---|---|---|---|---|
| **B3LYP/LANL2TZ** | | | | | | |
| VO$_2$H$^-$ | 4 | 1.905 | 1.657 | 0.956 | 144.1 | 0 |
| VO$_2$H | 3 | 1.841 | 1.611 | 0.955 | 155.9 | 0 |
| **BP86/LANL2TZ** | | | | | | |
| VO$_2$H$^-$ | 4 | 1.895 | 1.654 | 0.968 | 137.5 | 0 |
| VO$_2$H | 3 | 1.801 | 1.605 | 0.968 | 122.9 | 0 |

$^a$ The O$_\alpha$ is the oxygen atom which is adjacent to hydrogen atom. The O$_\beta$ is the oxygen atom on the other side. $^b$ Bond angle of OVO.

method and level that can better describe the electronic properties of hydride vanadium dioxide clusters. According to the present calculations, the theoretical EA of $VO_2H^-$ cluster are 1.390 and 1.332 eV for B3LYP and BP86 methods, respectively, which are listed in Table 3. The calculated EA values under two methods are in good agreement with experimentally measure data deviating by just 5% and 1% for that of $VO_2H^-$, respectively. This demonstrates that the level of theory and basis set used here is appropriate to predict the electronic properties of hydride vanadium dioxide clusters.

To get more insights in the molecular orbitals (MOs) and bonding of the anionic $VO_2H^-$ cluster, we have calculated the occupied valence Kohn–Sham MOs of the $VO_2H^{0/-1}$ clusters. As shown in Fig. 4, for both theoretical methods, there are 9 valence electronic MOs formed in the $VO_2H^-$ cluster, including 3 singly occupied MOs (HOMO–HOMO-2) on vanadium atom, 5 bonding orbitals (HOMO-3–HOMO-7) on V–O bond and one bonding orbital (HOMO-8) of O–H bond. The only difference between B3LYP and BP86 method is the energy order of $17a'$ and $16a'$. For B3LYP method, the single electron occupied HOMO ($17a'$) is mainly 4s character on vanadium atom, this orbital symmetry is very similar with the $10a_1$ orbital of the $VO_2^-$. Under BP86 method, the HOMO ($16a'$) is mainly $3d_{z^2}$ character on vanadium atom, this orbital symmetry is similar with the $4b_1$ orbital of the $VO_2^-$.[48,52] It means the singly occupied orbital symmetries of anionic $VO_2H$ is very similar with that of $VO_2^-$. From the shapes of bonding orbitals on V–O, it induces that the V–O bond is more ionic character since the charge density is mainly distributed on the oxygen atoms. As shown in B3LYP method, the extra electron was detached from single occupied HOMO ($17a'$) of the anionic $VO_2H$ to form the neutral cluster, supporting the experimentally observed $\beta$ value (1.63 ± 0.10) and the triplet character of the ground state of $VO_2H$.

**Table 4** The calculated vibrational frequencies of $VO_2H$ cluster in the neutral ground electronic state

| Method | Vibrational frequencies (cm$^{-1}$) | | | | | |
|---|---|---|---|---|---|---|
| | $\nu_1$ | $\nu_2$ | $\nu_3$ | $\nu_4$ | $\nu_5$ | $\nu_6$ |
| B3LYP | 80 | 417 | 440 | 690 | 1043 | 3940 |
| BP86 | 183 | 270 | 496 | 717 | 1022 | 3771 |

### Vibration assignments

Assignments are made based on the measured peak position and the calculated frequencies. The vibrational progressions in Fig. 2 are characteristic of the electronically distinct photodetachment transition, with four active vibrational modes in the neutral ground state of the cluster. As above calculation results, the anionic and neutral $VO_2H$ clusters are planner and bent asymmetrical structure, respectively. For neutral $VO_2H$ cluster, there are six active vibrational modes: $\nu_1$ OVO in-plane molecular bending vibration, $\nu_2$ OH out of plane bending vibration, $\nu_3$ OH in-plane bending vibration, $\nu_4$ V–OH stretching vibration, $\nu_5$ V–O stretching vibration and $\nu_6$ OH stretching vibration. The $\nu_2$ mode is inactive because both geometries of anionic and neutral cluster in the ground electronic state are planar. And the frequency of $\nu_6$ is out of the photoelectron detachment laser energy region. The calculated vibrational frequencies of the neutral ground electronic state by B3LYP and BP86 methods are listed in Table 4, respectively.

Peak X is assigned the vibrational origin of neutral ground state. Furthermore, the EAs are calculated to be 1.33 and 1.39 eV by the BP86 and B3LYP functional, respectively, in good agreement with the eBE of peak X at 1.304 eV. The first progression of ~100 cm$^{-1}$ consist of peaks X1–X3. The calculated frequency of the $\nu_1$ bending mode in the neutral ground state is 80 cm$^{-1}$, lies within 20 cm$^{-1}$ of this spacing (Table 1), so this set of peaks is
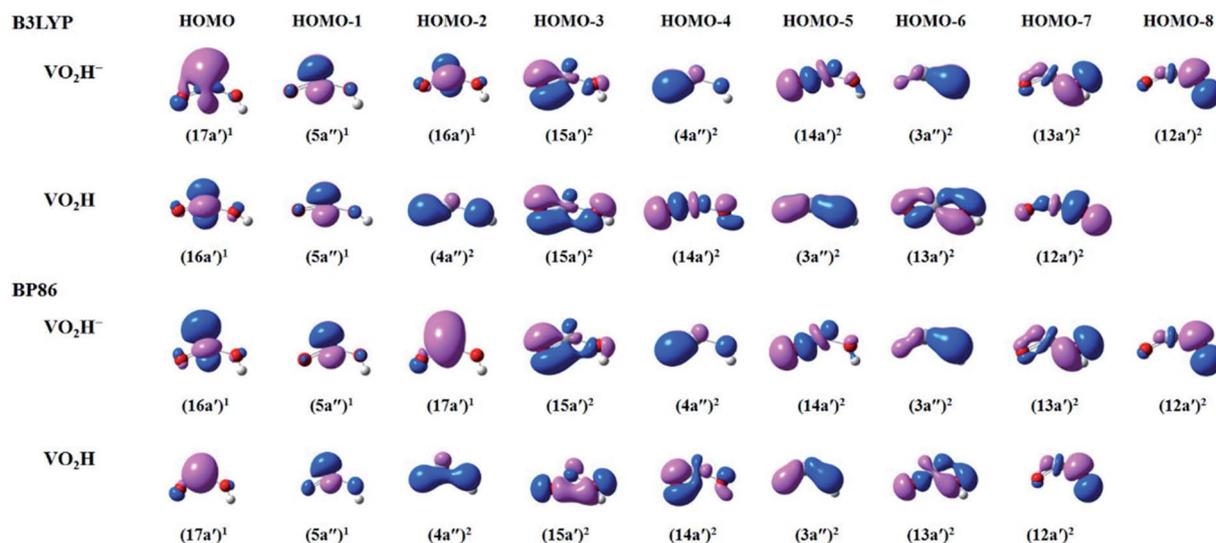


**Fig. 4** The plots of select occupied valence Kohn–Sham molecular orbitals (MOs) calculated by B3LYP (top) and BP86 (bottom) methods, describing the bonding in the anionic and neutral $VO_2H$ species.

assigned to $1_0^n$ ($n$ = 1–3) progression. Offset by 460 cm$^{-1}$ from the peak X is the series of peaks X4 and X5. The calculated $\nu_3$ OH in-plane bending vibration frequency is 440 cm$^{-1}$ for the neutral ground state, so this second series of peaks is assigned to the $1_0^n 3_0^1$ ($n$ = 0–1) progression. The third progression, which is offset by 734 cm$^{-1}$ from the vibrational origin, consist of peaks X6–X8. The peaks spacing is about 60 cm$^{-1}$. The calculated $\nu_4$ V–OH stretching vibration frequency is 690 cm$^{-1}$, so this series of peaks is assigned to the $1_0^n 4_0^1$ ($n$ = 0–2) progression. The fourth progression, which consists of peaks X9–X11, is offset by 1065 cm$^{-1}$ from the vibrational origin band. This value is in close agreement with the calculated frequency for $\nu_5$ V–O stretching vibration, which is 1043 cm$^{-1}$, so this series of peaks is assigned to the $1_0^n 5_0^1$ ($n$ = 0–2) progression. The assigned EAs, adiabatic term energies, and vibrational frequencies are summarized in Table 1.

### Franck–Condon simulations

According to the B3LYP method the singly occupied HOMO orbital is mainly 4s character on vanadium atom. Under BP86 method, the HOMO orbital is mainly 3d$_{z^2}$ character on vanadium atom. It means that the two methods give the different electronic configuration for the VO$_2$H$^-$ ground state. It is difficult to confirm the electronic configuration by calculated EA values, because those values obtained from two methods are all close to the experimental value. Although the experimental $\beta$ value support the results of B3LYP, it is still not a sufficient condition.

To aid in the assignment of the photodetachment transitions, particularly the identification of the anion ground state, FC simulations are calculated from the two quartet anion states to the triplet neutral states. B3LYP and BP86 give different geometry changes upon electron detachment, thus the calculated FC spectra should be discriminatory with the results from either method. Both B3LYP and BP86 geometries, normal
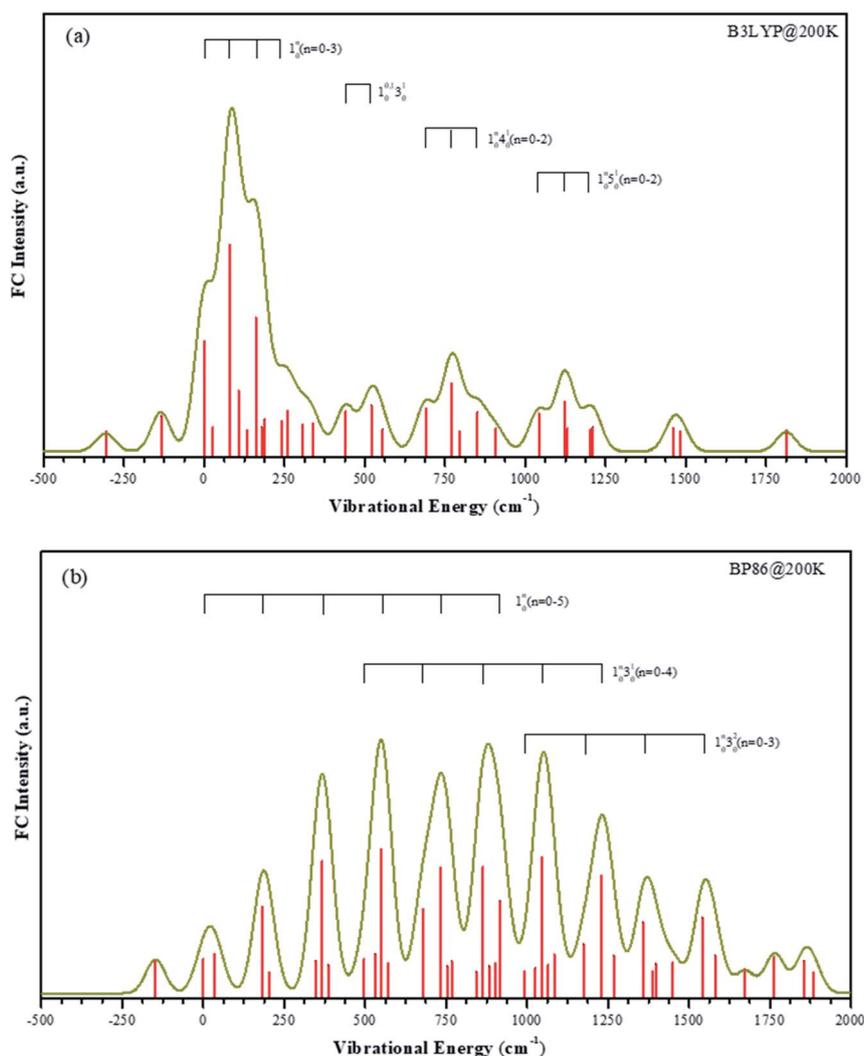


**Fig. 5** Calculated FC intensities for the transitions from the anion ground electronic states to the neutral ground electronic states of VO$_2$H at about 200 K, the dark yellow line is the simulated spectra curves. Panel (a) is the simulated spectra using vibrational frequencies calculated by B3LYP method. Panel (b) is the simulated spectra using vibrational frequencies calculated by BP86 method.

modes, and vibrational frequencies are used for an internally consistent set of FC simulations. FC simulations are generated using the ezSpectrum program,[53] which calculates FC intensities in the harmonic oscillator approximation but with full Duschinsky mixing of the normal modes.[54]

The temperature in our molecular beam was estimated at about 200 K by FC simulation. The spectra curves of calculated FC intensities are displayed in Fig. 5, showing simulated detachment spectra from the quartet anion state to the triplet neutral state. All geometries, vibrational frequencies, and normal mode coordinates are those calculated at both B3LYP/LANL2TZ and BP86/LANL2TZ levels to make comparison. The horizontal scale is internal energy within a given electronic state, thus all vibrational origins are set to zero energy.

The FC profiles support the choice of the electronic state calculated by B3LYP method as the anion ground state. As shown in the experimental spectrum, there are four series vibrational progressions. The offsets from the original band are $105$ $cm^{-1}$, $460$ $cm^{-1}$, $734$ $cm^{-1}$ and $1065$ $cm^{-1}$, respectively. Under the B3LYP level, the FC profiles are in good agreement with the characters in the experimental bands, and the frequency lies within $30$ $cm^{-1}$ of the offset. The simulated four vibrational progressions are offset by $81$ $cm^{-1}$, $440$ $cm^{-1}$, $690$ $cm^{-1}$ and $1043$ $cm^{-1}$, corresponding to the $\nu_1$, $\nu_2$, $\nu_3$ and $\nu_4$ active modes, respectively. In the spectrum, the experimental $1_0^n$ ($n = 1$–3) progression peak in intensity $n = 1$. The most intense transition in the simulated band by B3LYP level is also the $1_0^1$ transition, while under BP86 method, this simulated band is assigned at $1_0^3$ transition, which is offset by $550$ $cm^{-1}$. In the experimental result, the frequency of hot band X′ is less than original band X by $137$ $cm^{-1}$, which is the frequency of $\nu_1$ mode in the anionic ground state. Thus, frequency of $\nu_1$ mode in the $VO_2H^-$ ground state is larger than in its corresponding neutral ground state. The simulated frequencies of $1_1^0$ and $1_0^1$ are $135$ $cm^{-1}$ and $81$ $cm^{-1}$ under B3LYP level, respectively. However, under BP86 level, these two values are $149$ $cm^{-1}$ and $183$ $cm^{-1}$, respectively. Obviously, the results given by B3LYP method is agreement with that in experiment.

According to the FC simulated profiles, we assigned the electronic configuration of anion ground state by B3LYP method. Henceforth refer to the single electron occupied HOMO orbital of $VO_2H^-$ is mainly 4s character on vanadium atom, which is similar with the $10a_1$ orbital of the $VO_2^-$.

## 4. Conclusion

In conclusion, from the changes in mass spectrum when trace ethanol was carried, we induced that the $VO_2^-$ combined very easily with the hydrogen atom in the ethanol to form $VO_2H^-$. The photoelectron imaging spectrum of anionic $VO_2H$ cluster was firstly reported at a photon energy of 1.52 eV (815 nm). The observed PES possesses obvious vibrational structures, from which the EA of $VO_2H$ was measured to be $1.304 \pm 0.030$ eV and VDE was $1.317 \pm 0.030$ eV. The $\nu_1$, $\nu_3$, $\nu_4$ and $\nu_5$ vibrational frequencies are also obtained for the ground state of neutral $VO_2H$. The calculated energetics, FC profiles and observed PADs ($\beta$ value), vibrational peaks all suggest that the ground state of

$VO_2H^-$ is $X\,^4A''$ with the highest single occupied MO is mainly 4s components rather than 3d component on vanadium atom. Even relatively simple transition metal systems, such as neutral and anion $VO_2H$, can have several uncertain electronic configurations, and disentangling them requires careful analysis by different theoretical methods, FC simulation and combining with the high-resolution experimental technique. Comparing with the accomplished level for main group chemistry, the theoretical methods of transition metal computational chemistry are still being developed. The electron VIM technique is still useful to explore the HOMO shape and is aided to assign the electronic configuration in this cluster system.

## Conflicts of interest

There are no conflicts to declare.

## Acknowledgements

## Notes and references

1 B. M. Weckhuysen and D. E. Keller, *Catal. Today*, 2003, **78**, 25–46.

2 G. C. Bond and S. F. Tahir, *Appl. Catal.*, 1991, **71**, 1–31.

3 M. Baltes, *Synthesis and characterization of vanadium oxide catalysis*, 2003.

4 B. Grzybowska-Świerkosz, *Appl. Catal., A*, 1997, **157**, 263–310.

5 G. Deo, I. Wachs and J. Haber, *Crit. Rev. Surf. Chem.*, 1994, **4**, 141–187.

6 H. Knözinger and J. Weitkamp, *Handbook of heterogeneous catalysis*, 1997, vol. 3.

7 N. Armaroli and V. Balzani, *Angew. Chem., Int. Ed.*, 2007, **46**, 52–66.

8 G. Centi, F. Cavani and F. Trifirò, *Selective oxidation by heterogeneous catalysis*, Springer Science & Business Media, 2012.

9 D. Schröder, M. Engeser, H. Schwarz, E. C. E. Rosenthal, J. Döbler and J. Sauer, *Inorg. Chem.*, 2006, **45**, 6235–6245.

10 D. Schröder, J. Loos, M. Engeser, H. Schwarz, H.-C. Jankowiak, R. Berger, R. Thissen, O. Dutuit, J. Döbler and J. Sauer, *Inorg. Chem.*, 2004, **43**, 1976–1985.

11 L. Zhao, M. Tan, J. Chen, Q. Ding, X. Lu, Y. Chi, G. Yang, W. Guo and Q. Fu, *J. Phys. Chem. A*, 2013, **117**, 5161–5170.

12 J. Döbler, M. Pritzsche and J. Sauer, *J. Am. Chem. Soc.*, 2005, **127**, 10861–10868.

13 A. Fielicke, R. Mitrić, G. Meijer, V. Bonačić-Koutecký and G. von Helden, *J. Am. Chem. Soc.*, 2003, **125**, 15716–15717.

14 P. Boulet, A. Baiker, H. Chermette, F. Gilardoni, J. C. Volta and J. Weber, *J. Phys. Chem. B*, 2002, **106**, 9659–9667.

15 N. A. Moore, R. Mitrić, D. R. Justes, V. Bonačić-Koutecký and A. Castleman, *J. Phys. Chem. B*, 2006, **110**, 3015–3022.

16 M. Engeser, D. Schröder and H. Schwarz, *Eur. J. Inorg. Chem.*, 2007, 2454–2464.

17 M. Engeser, D. Schröder and H. Schwarz, *Chem.–Eur. J.*, 2005, **11**, 5975–5987.

18 S. Feyel, L. Scharfenberg, C. Daniel, H. Hartl, D. Schröder and H. Schwarz, *J. Phys. Chem. A*, 2007, **111**, 3278–3286.

19 T. Waters, A. G. Wedd and R. A. J. O'Hair, *Chem.–Eur. J.*, 2007, **13**, 8818–8829.

20 F. Dong, S. Heinbuch, Y. Xie, J. J. Rocca and E. R. Bernstein, *J. Phys. Chem. A*, 2009, **113**, 3029–3040.

21 D. R. Justes, N. A. Moore and A. W. Castleman, *J. Phys. Chem. B*, 2004, **108**, 3855–3862.

22 Y. Cao, X. Zhao, B. Xin, S. Xiong and Z. Tang, *J. Mol. Struct.: THEOCHEM*, 2004, **683**, 141–146.

23 T. Feng and J. Vohs, *J. Phys. Chem. B*, 2005, **109**, 2120–2127.

24 L. A. Gambaro, *J. Mol. Catal. A: Chem.*, 2004, **214**, 287–291.

25 T. Waters, G. N. Khairallah, S. A. Wimala, Y. C. Ang, A. Richard and A. G. Wedd, *Chem. Commun.*, 2006, 4503–4505.

26 J. B. Kim, M. L. Weichman and D. M. Neumark, *J. Chem. Theory Comput.*, 2014, **10**, 5235–5237.

27 M. F. A. Hendrickx and V. T. Tran, *J. Chem. Theory Comput.*, 2014, **10**, 4037–4044.

28 S. F. Vyboishchikov and J. Sauer, *J. Phys. Chem. A*, 2000, **104**, 10913–10922.

29 H. Wu and L.-S. Wang, *J. Chem. Phys.*, 1998, **108**, 5310–5318.

30 J. B. Kim, M. L. Weichman and D. M. Neumark, *J. Chem. Phys.*, 2014, **140**, 034307.

31 Y.-T. Wang, C.-C. Han, Z.-J. Fei, C.-W. Dong and H.-T. Liu, *J. Phys. Chem. A*, 2020, **124**, 5590–5598.

32 W. Wiley and I. H. McLaren, *Rev. Sci. Instrum.*, 1955, **26**, 1150–1157.

33 B. Dick, *Phys. Chem. Chem. Phys.*, 2014, **16**, 570–580.

34 J. Ho, K. M. Ervin and W. Lineberger, *J. Chem. Phys.*, 1990, **93**, 6987–7002.

35 M. J. Frisch, G. W. Trucks, H. B. Schlegel, G. E. Scuseria, M. A. Robb, J. R. Cheeseman, G. Scalmani, V. Barone, B. Mennucci and G. A. Petersson, *et al.*, *Gaussian 09, Revision A.1*, Gaussian, Inc., Wallingford, CT, 2009.

36 A. D. Becke, *Phys. Rev. A: At., Mol., Opt. Phys.*, 1988, **38**, 3098–3100.

37 J. P. Perdew, *Phys. Rev. B: Condens. Matter Mater. Phys.*, 1986, **33**, 8822–8824.

38 A. D. Becke, *J. Chem. Phys.*, 1993, **98**, 5648–5652.

39 T. H. Dunning Jr, *J. Chem. Phys.*, 1989, **90**, 1007–1023.

40 P. J. Hay and W. R. Wadt, *J. Chem. Phys.*, 1985, **82**, 299–310.

41 L. E. Roy, P. J. Hay and R. L. Martin, *J. Chem. Theory Comput.*, 2008, **4**, 1029–1031.

42 J. Cooper and R. N. Zare, *J. Chem. Phys.*, 1968, **48**, 942–943.

43 K. L. Reid, *Annu. Rev. Phys. Chem.*, 2003, **54**, 397–424.

44 S. J. Peppernick, K. D. D. Gunaratne and A. W. Castleman Jr, *Proc. Natl. Acad. Sci. U. S. A.*, 2010, **107**, 975–980.

45 A. J. Mere, *Annu. Rev. Phys. Chem.*, 1989, **40**, 407–438.

46 K. R. Asmis, G. Meijer, M. Brümmer, C. Kaposta, G. Santambrogio, L. Wöste and J. Sauer, *J. Chem. Phys.*, 2004, **120**, 6461–6470.

47 M. F. A. Hendrickx and V. T. Tran, *J. Chem. Theory Comput.*, 2014, **10**, 4037–4044.

48 J. B. Kim, M. L. Weichman and D. M. Neumark, *J. Chem. Phys.*, 2014, **140**, 0343071–0343079.

49 S. F. Vyboishchikov and J. Sauer, *J. Phys. Chem. A*, 2000, **104**, 10913–10922.

50 M. Pykavy and C. van Wüllen, *J. Phys. Chem. A*, 2003, **107**, 5566–5572.

51 J. F. Harrison, *Chem. Rev.*, 2000, **100**, 679–716.

52 J. B. Kim, M. L. Weichman and D. M. Neumark, *J. Chem. Theory Comput.*, 2014, **10**, 5235–5237.

53 V. A. Mozhayskiy and A. I. Krylov, *ezSpectrum*, 2009, see http://iopenshell.usc.edu/downloads.

54 F. Duschinsky, *Acta Physicochim. URSS*, 1937, **7**, 551.

55 Y.-L. Li, X.-G. Xiong and H.-T. Liu, *Nucl. Sci. Tech.*, 2019, **30**(5), 70.